Available online at www.sciencedirect.com
ScienceDirect
Optics Communications 274 (2007) 50–58
OPTICS COMMUNICATIONS
www.elsevier.com/locate/optcom

Unified approach to short optical pulse recording and spatial imaging with subwavelength resolution

Naum K. Berger *, Baruch Fischer

Technion – Israel Institute of Technology, Department of Electrical Engineering, 32000 Haifa, Israel

Received 18 June 2006; received in revised form 20 January 2007; accepted 30 January 2007

Abstract

We propose and numerically demonstrate a simple method for measuring waveforms of optical pulses that have spectral bandwidths much larger than the passband of the measuring system, thus enabling a kind of temporal superresolution. The technique is based on pulse intensity modulation that contains high-order harmonics. Parts of the pulse intensity spectrum that are shifted as a result of the modulation, are moved over (''umklapped'') to the center of the passband, transmitted and then recorded by an oscilloscope. The pulse intensity spectrum is restored by parts from the Fourier transform of a few oscillograms, measured after performing the temporal shifts between the pulse train and the modulation. A similar approach is applied for achieving subwavelength spatial resolution in far – field microscopy. The spatial modulation is performed by a diffraction grating. The method allows one to restore a subwavelength object in a single measurement.

PACS: 42.30.−d; 42.30.Lr; 42.65.Re

Keywords: Optical pulses; Temporal imaging; Temporal superresolution; Spatial imaging; Subwavelength resolution

1. Introduction

Monitoring of optical pulse waveforms with picosecond temporal resolution is important for next generation of optical communication systems operating at a data rate of 40 Gb/s, as well as for other applications, such as time-resolved spectroscopy, material processing, etc. A simple and widely used direct measurement of pulse waveforms is done with fast photodiodes and sampling oscilloscopes. However, their available bandwidth is presently below 50–70 GHz. One of the possible ways to overcome this barrier is temporal imaging in which the pulse is temporally magnified [1,2], similarly to spatial magnification by microscopes, or alternatively converted to the spectral domain while keeping the shape (spectro-temporal imaging) [3–5]. Such methods are based on the time–space analogy, where time lenses (phase modulators) and dispersion are analogs of regular spatial lenses and free space diffraction. Time lenses can be practically implemented using an electrooptic phase modulator [2,3,5], or by mixing the objective pulse with a chirped pulse in a non-linear crystal by sum-frequency generation [1], or by cross-phase modulation in a non-linear fiber [4]. Temporal imaging imposes certain conditions on the phase modulation and the dispersive elements: The temporal dependence of the modulation phase and the spectral phase response of the dispersive elements have to be close to quadratic in order to avoid temporal aberrations of the pulses, and the dispersion magnitudes and modulation amplitude ought to be matched. Additionally, non-linear temporal imaging requires relatively high light intensities.

In this paper we present a simple method for optical pulse measurements by photodiodes and oscilloscopes with passbands that are much narrower than the pulse bandwidth. The technique is based on periodic pulse modulation, which provides high-order harmonics. There are no other basic requirements, such as dispersive elements that

* Corresponding author. Tel.: +972 48294736; fax: +972 48295757.
E-mail address: chrberg@techunix.technion.ac.il (N.K. Berger).

0030-4018/$ - see front matter © 2007 Elsevier B.V. All rights reserved.
doi:10.1016/j.optcom.2007.01.073

are needed in temporal imaging, where the pulse to be measured is stretched and its intensity spectrum, the Fourier transform of the pulse intensity, is accordingly compressed in order to be transmitted through the passband of a diode and an oscilloscope. In our technique, the pulse spectrum is divided into a certain number of parts. Each part is spectrally shifted owing to the modulation, moved into the passband (''umklapped''), transmitted and restored after processing of the oscilloscope traces. Thus, the whole pulse intensity spectrum and then the pulse waveform are restored. The method that is entirely linear and therefore can by used for low pulse intensities, is demonstrated by numerical simulations for single shots and periodic pulses. We also show that the same approach can be applied for the spatial case, obtaining a subwavelength resolution in conventional far-field microscopy. The temporal modulation is replaced in this case by spatial modulation with a periodic diffraction grating.

In this way we demonstrate, for the first time to the best of our knowledge, a close analogy between spatial and temporal superresolution, and methods for achieving it.

2. Measurement principle

The basis of our method is periodic intensity modulation of the pulse to be measured. A periodic modulation function $f_m(t)$ can be expanded into a Fourier series

$$f_m(t) = \sum_{n=-N}^{N} c_n \exp(in\omega_m t), \tag{1}$$

where c_n are the Fourier coefficients, $\omega_m = 2\pi/T_m$, T_m is the modulation period, and the number of non-zero modulation harmonics is $2N+1$. The pulse intensity at the modulator output has the form

$$I_{out}(t) = I_{in}(t) \sum_{n=-N}^{N} c_n \exp(in\omega_m t), \tag{2}$$

where $I_{in}(t)$ is the input pulse intensity. Assuming that the measured photodiode signal is proportional to the optical pulse intensity, we can introduce the optoelectronic transfer function (OETF) $H(\omega)$ as a ratio of the spectrum of the output oscilloscope signal and the spectrum of the input pulse intensity [6]. $H(\omega)$ describes the spectral characteristics of the photodiode and the oscilloscope together. If we take into account negative frequencies, the function $H(\omega)$ ought to be continued in this region with the condition $H(-\omega) = H^*(\omega)$, where $*$ denotes complex conjugation. The Fourier transform of (2) gives the spectrum of the oscilloscope output signal (in arbitrary units):

$$V(\omega) = H(\omega) \sum_{n=-N}^{N} c_n F_{in}(\omega - n\omega_m), \tag{3}$$

where $F_{in}(\omega)$ is the intensity spectrum of the input optical pulse.

We assume that the pulse spectrum bandwidth is much larger than the bandwidth of the OETF. In the absence of modulation, the series in (3) has a single term with $n = 0$. The input pulse spectrum has a cutoff imposed by the transfer function and then the information imbedded in the high-frequency spectral components is lost. The pulse on the oscilloscope screen will be much wider than the original input pulse. As can be seen from (3), owing to periodic modulation, we obtain a sum of shifted spectra of the pulse intensity. We assume that for the Nth shifted spectrum (and similarly for $-N$) the intensity that is comparable to the noise level lies within the spectral region with non-zero transfer function. It implies that now the whole information about the pulse intensity spectrum is included in its $2N+1$ parts that can be transmitted by a photodiode and an oscilloscope with a certain weight. In this case, the pulse on the oscilloscope screen will also be much wider than the input pulse, but its Fourier transform contains information about the whole pulse intensity spectrum and it can be extracted. It is desirable to choose the modulation frequency $\omega_m/(2\pi)$ to be close to the full width of the complex OETF. We denote the anticipated full width of the input pulse spectrum by W. Then the number of the needed harmonics can be estimated as

$$2N + 1 = \frac{2\pi W}{\omega_m}.$$

One of the ways for extracting the information is to record $2N+1$ oscillograms for the different temporal shifts between the input optical pulse train and the intensity modulation. (For another way with a single recording, see below at the spatial analog.) Spatial shifts for similar purposes were used in fluorescence microscopy with structured illumination [7–9]. Eq. (3) can be rewritten as

$$V_k(\omega) = H(\omega) \sum_{n=-N}^{N} c_n \exp(in\omega_m \tau_k) F_{in}(\omega - n\omega_m), \tag{4}$$

where τ_k is the kth temporal shift, $k = 1, \ldots, 2N+1$. Eq. (4) gives a set of linear equations for $2N+1$ unknown functions $F_{in}(\omega - n\omega_m)$. $V_k(\omega)$ can be found from the Fourier transform of the kth experimental oscillogram. The Fourier coefficients, c_n, of the modulation function have to be measured as well. Each obtained spectrum $F_{in}(\omega - n\omega_n)$ is shifted back to the original place in the spectrum. Once the whole spectrum of the input pulse is reconstructed, the pulse intensity is calculated using a Fourier transform.

3. Recording short optical pulses

In our simulations for the pulse waveform measurement, we studied two different cases: (a) The first one is for pulse repetition rates that are much smaller than the modulation frequency. Then, the pulse intensity spectrum can be considered as continuous compared with the discrete modulation spectrum and the data processing can be performed as

for a single pulse. It is clear that in reality high speed sampling oscilloscopes can measure only periodic pulses. (b) In the second case, the pulse repetition rate and the modulation frequency are equal. We show below that this condition substantially simplifies the measurement and the processing. There is even no necessity to use an oscilloscope in this case; only an intensity modulator and a power meter are required for the periodic pulse waveform measurement.

3.1. Single pulse

We assume that the intensity modulation is performed by a Mach–Zehnder modulator and the modulation function can be written as

$$f_{\mathrm{m}}(t) = |1 + \exp\{\mathrm{i}\varphi_0 + \mathrm{i}A\sin[\omega_{\mathrm{m}}(t-\tau_k)]\}|^2, \tag{5}$$

where A is the modulation index and φ_0 is the constant phase. We expand (5) into a Fourier series with the coefficients

$$\begin{aligned} c_0 &= 2 + 2J_0(A)\cos(\varphi_0), \\ c_n &= [\exp(\mathrm{i}\varphi_0) + (-1)^n \exp(-\mathrm{i}\varphi_0)]J_n(A), \quad n \neq 0, \end{aligned} \tag{6}$$

where $J_n(A)$ is the n-order Bessel function of the first kind. We chose here $\varphi_0 = 0$. Then, it can be seen from (6) that the modulation has only even harmonics.

The optical pulse was assumed to be Gaussian with a full width at half maximum (FWHM) of 2.5 ps. The original pulse is shown in Fig. 1 (solid curve). The intensity spectrum of this pulse is shown in Fig. 2 (solid curve). The spectrum width (FWHM) is 353 GHz. We show also in this figure the Gaussian optoelectronic transfer function $H(\omega)$ of the oscilloscope–photodiode system that is used in the simulations (dashed curve). Its half-width (the width of the real transfer function) is 50 GHz. Since the pulse bandwidth is much larger than the passband of the system, the pulse recorded by an oscilloscope without any processing would be broadened in comparison with the original pulse, as shown in Fig. 1 (dashed curve). We used the following parameters of the pulse modulation: $f_{\mathrm{m}} = 40$ GHz, $A = 2\pi$. Note that the even modulation harmonics give in this case a frequency shift $\Delta f = 2f_{\mathrm{m}} = 80$ GHz. The number N that corresponds to that modulation and the pulse spectrum was taken to be 5.

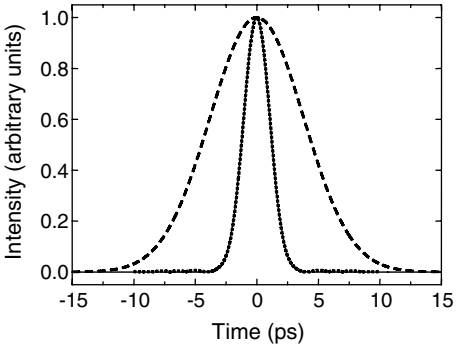

Fig. 1. Intensity profiles of the original pulse (solid curve) with FWHM of 2.5 ps and the restored pulse (dotted curve). The oscillogram of this pulse (dashed curve) that would be recorded by a photodetector and an oscilloscope with 50 GHz width of an OETF.

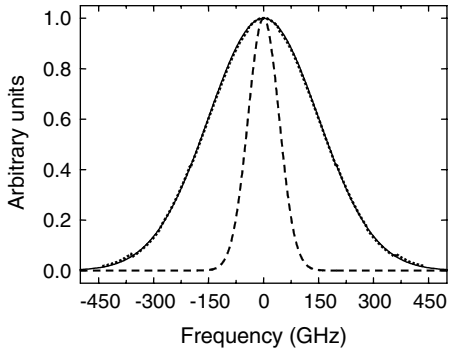

Fig. 2. Original (solid curve) and restored (dotted curve) spectra of the pulses shown in Fig. 1. The OETF (dashed curve) of a photodetector and an oscilloscope with a 50 GHz width for positive frequencies.

In simulating the experiment, we obtained $2N + 1 = 11$ oscillograms, shifting each time the modulating signal by $\Delta\tau = 0.4$ ps ($\tau_k = k\Delta\tau$). The Fourier transform $V_k(\omega)$ of the kth oscillogram was substituted to Eq. (4). The solution for each sampling point ω_i gives $2N + 1 = 11$ values of the shifted spectrum parts $F_{\mathrm{in}}(\omega_i - n\omega_{\mathrm{m}})$ ($n = -5, \ldots 0, \ldots 5$), shown in Fig. 3. The original pulse intensity spectrum is reconstructed by shifting each spectrum part $F_{\mathrm{in}}(\omega_i - n\omega_{\mathrm{m}})$ to its original place in the spectrum. The restored spectrum is shown in Fig. 2 (dotted curve). One can see the excellent agreement between the original and restored spectra. The curves almost coincide. The Fourier transform of the restored spectrum gives the restored pulse shown in Fig. 1 (dotted curve). We also see here again the excellent reconstruction of the original waveform.

3.2. Periodic pulses

A periodic pulse train was obtained by simulating sinusoidal phase modulation of cw light with a frequency of 40 GHz and a modulation index of 3.8 rad. The modulated light was then propagated through a fiber with dispersion of 2.8 ps/nm. The calculated pulses at the fiber output are shown in Fig. 4 (solid curve). The pulse width (FWHM)

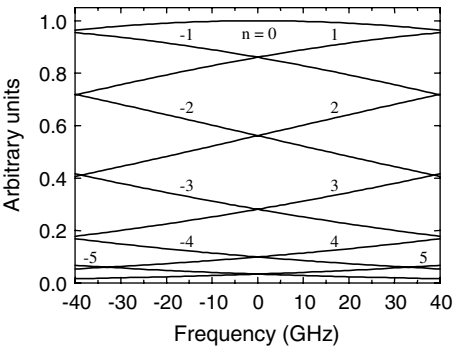

Fig. 3. Restored shifted parts $F_{\mathrm{in}}(\omega - n\omega_{\mathrm{m}})$ of the pulse spectrum within the frequency interval (−40 GHz, 40 GHz).

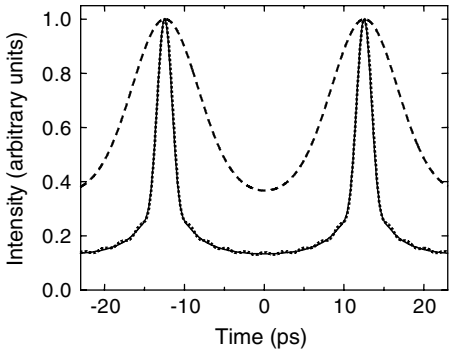

Fig. 4. Original periodic pulses (solid curve) with a repetition rate of 40 GHz and FWHM of 2.66 ps and restored pulses (dotted curve). The oscillogram of these pulses (dashed curve) that would be recorded by a photodetector and an oscilloscope with a 50 GHz width of the OETF (in the absence of the second modulation).

is 2.66 ps. The discrete spectrum (Fourier coefficients) of the pulse intensity is presented in Fig. 5 (squares). The modulation parameters were the same as those taken for the single pulse calculation, except that $\varphi_0 = 3.9$ rad. The frequency shift was $\Delta f = f_m = 40$ GHz and $N = 10$. Fig. 6 shows the spectrum of the modulation harmonics.

The periodic pulse intensity can be expressed as a Fourier series

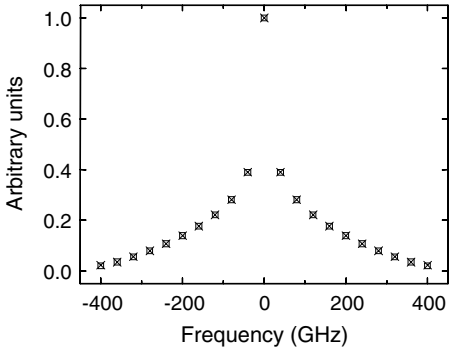

Fig. 5. Discrete intensity spectrum (Fourier coefficients) of the original (squares) and restored (crosses) periodic pulses shown in Fig. 4.

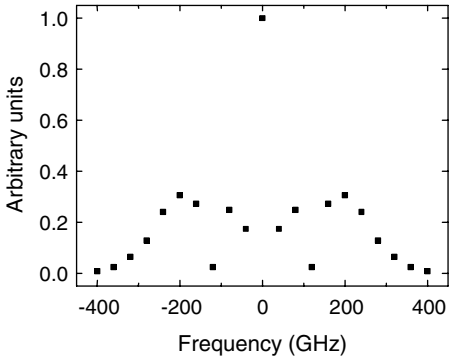

Fig. 6. Spectrum (Fourier coefficients) of the periodic intensity modulation with a frequency of 40 GHz.

$$I_{\text{in}}(t) = \sum_{n=-N}^{N} b_n \exp(\mathrm{i}n\omega_{\text{m}}t), \tag{7}$$

where b_n are the Fourier coefficients and $2N+1$ is the number of non-zero harmonics. Using (1) and (7), we can obtain for the intensity of the modulated pulses:

$$I_{\text{mod}}(t) = I_{\text{in}}(t) f_{\text{m}}(t) = \sum_{n=-2N}^{2N} \sum_{l=-N}^{N} c_l b_{n-l} \exp(-\mathrm{i}l\omega_{\text{m}}\tau) \exp(\mathrm{i}n\omega_{\text{m}}t), \tag{8}$$

where τ is the time delay between the original pulse and the modulation function. The intensity shape of the recorded pulses depends on the OETF of a measurement system.

We first assume the simplest case when the width of the OETF is close to 0, much less than the modulation frequency. It can be implemented, for instance, by measuring the modulated pulse intensity with a dc power meter, instead of an oscilloscope. In this case, only the term $n = 0$ remains in the sum in (8) for the recorded pulses. Thus, we obtain from (8), the power P_k measured (in arbitrary units) after the kth temporal shift ($k = -N, \ldots 0, \ldots, N$)

$$P_k = \sum_{l=-N}^{N} c_l b_{-l} \exp(-\mathrm{i}l\omega_{\text{m}}\tau_k). \tag{9}$$

Expression (9) can be treated as a set of $2N+1$ equations for $2N+1$ unknown Fourier coefficients b_l. Solving this system and using Eq. (7), we obtain the original pulse waveform.

We made simulations for the periodic pulses shown in Fig. 4. Fig. 7 shows $2N+1 = 21$ values of the calculated averaged power P_k for temporal shifts $\tau_k = k\Delta\tau$, $\Delta\tau = 1.2$ ps. The restored Fourier coefficients b_l are presented in Fig. 5 (crosses); they fully coincide with the values of the original pulses. The restored pulse intensity is shown in Fig. 4 (dotted curve) along with the original pulses, for comparison. One can see excellent agreement. We emphasize again that our method becomes very simple for periodic pulse waveform measurements, when the modulation frequency is equal to the pulse repetition rate. It requires only $2N+1$ shifts between the modulation and the pulse

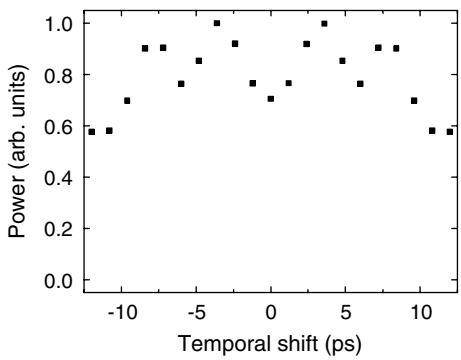

Fig. 7. Values of the average power of the modulated periodic pulses for the different temporal shifts between the pulse train and the modulation.

train and $2N+1$ measurements of the average powers by a simple power meter. These measurements and the processing can be carried out in real time and displayed on a computer screen. We should also note that an implementation needs high-quality synchronization between the measured pulses and the modulation: it can be done by using an amplified portion of the detected pulses.

The measurements can also be done with a photodiode and an oscilloscope. For a real OETF width of 50 GHz, the calculated oscillogram of the original pulses (in the absence of the second modulation) is shown in Fig. 4 (dashed curve).For the modulated pulses, only five intensity harmonics from (8) with $n=0,\pm1,\pm2$ would be recorded on the oscilloscope screen. In the data processing, the Fourier coefficients of $2N+1$ oscillograms of the modulated pulses have to be calculated. According to Eq. (8), the zeroth-order Fourier coefficients ($n=0$) give the same set of equations as presented in (9). The only difference is that the average power of the modulated pulses is now measured (in arbitrary units) not by a power meter, but by a photodiode and an oscilloscope. Analogous equations can be formulated, according to Eq. (8), calculating the first-order ($n=\pm1$) or the second-order ($n=\pm2$) Fourier coefficients of $2N+1$ oscillograms. If we write the equations for two or more orders together, the number of the temporal shifts can be accordingly decreased.

Our technique allows one to measure optical pulse waveforms even in the cases when their bandwidth is much larger than the width of the OETF, or in other words when the temporal resolution of a photodetector and an oscilloscope is insufficient. It can be said that our method effectively enhances their resolution. The enhancement depends on the modulation frequency and the modulation index. We took in the simulations parameters that represent the best commercial modulators. The bandwidth of the measuring devices (oscilloscope and photodetector) is effectively increased from 50 to 250 GHz that corresponds to measuring 2.5 ps width pulses. For the subpicosecond range, the modulators performance ought to be enhanced. For instance, modulation frequency of 75 GHz and modulation index of 7.5π can provide measurement of 500 fs width pulses.

The resolution of temporal imaging with a time lens (by an electrooptic modulator) is estimated in [10] as $\delta t \approx 1/\Delta F_{\mathrm{m}}$, where ΔF_{m} is the bandwidth of the modulation spectrum. The shortest pulse that can be measured by our method has the same spectral width as the modulation. For our case, $1/\Delta F_{\mathrm{m}}$ is the temporal duration of the pulse, meaning that our method provides at least the resolution of temporal imaging with a time lens. Then we have the advantage of the superresolution method that it does not need any dispersive element and does not impose any condition on the modulation function beside the existence of high-order harmonics.

Our method does not give complete characterization of optical pulses since it measures only the pulse intensity, and not the phase profile that is of interest, for example when studying non-transform-limited pulses. However, from the measured intensity of a temporal interference pattern one can extract information about the pulse phase profile by standard processing methods. It should be pointed out that the temporal resolution of an oscilloscope is determined not only by its transfer function, but also by the resolution of its time base, that has to be matched as well. The time base, for instance, of a 50 GHz oscilloscope has a resolution of up to 64 fs, but its accuracy is worse.

4. Spatial imaging with subwavelength resolution

The method described here can also be applied to subwavelength resolution in the spatial imaging case. The spatial spectrum of any object that can be transmitted by an optical imaging system is limited, as in the time domain, by its transfer function. The maximal transmitted spatial frequency determines the spatial resolution of a system. Two different objects having the same spatial spectrum within the passband of an optical system give indistinguishable identical images. The image ambiguity [11] holds when there is no a priori information about the objects. However, knowledge, for instance that the object has finite size, makes it possible to find the extension of the spatial spectrum beyond the system passband and reconstruct the object unambiguously [11]. Thus the classical resolution limit can be exceeded, thus giving spatial superresolution. The achievable resolution in this case is limited by noise [12]. A more general principle was established in [13]: the number of degrees of freedom of an optical message transmitted by an optical system is invariant. It allows, for instance, extending the bandwidth of transferred spatial frequencies above the classical value by reducing the bandwidth of transferred temporal frequencies [13]. Such an experimental demonstration was given in [14] where two gratings, inserted into the object and the image planes, moved synchronously in opposite directions and the image was temporally integrated by a photodetector. This method was further improved [15] by using Dammann gratings instead of Ronchi gratings that were used in [14].

The spatial spectrum of propagating light waves is limited in the range $(-1/\lambda,\ 1/\lambda)$, where λ is the wavelength. Therefore, the maximal resolution achievable in conventional far-field microscopy is about of $\lambda/2$. This limitation can also be viewed by the Heisenberg uncertainty principle [16]. The information about subwavelength details of an object is carried by evanescent waves that do not propagate from the object, but decay over distances comparable with the wavelength.

However, evanescent waves can be transformed to propagating waves, for instance by coupling to a tip in optical tunneling microscopy and in such a manner subwavelength details can be resolved. In far-field imaging such transformation can be performed by a diffraction grating [17], where the diffracted evanescent waves have a shifted spatial spectrum. If this spectrum lies within the optical transfer function (OTF) of an imaging system, the waves propagate

and can be recorded. In [17], an image of an object-grating with period of 380 nm was obtained in this way. The opposite transformation, from propagating to evanescent waves, is also possible by a diffraction grating, when the grating period is smaller than $\lambda/2$. Two diffraction gratings with equal [18] or close [19] subwavelength periods, rotated relative to each other, can be used for imaging one of them. In this case, the first grating serves as the object and produces the evanescent waves diffracted by the second grating, giving propagating waves with a spatial spectrum lying within the OTF of the optical system. For the decoding of the spatial information, an additional diffraction grating was used [19,20]. Recently, a novel near-field imaging system was proposed [21] in which a diffractive element may be translated relative to the object, where the distance between them ought to be kept as $\lambda/100$. It was though pointed out [19] that it is difficult to perform such a movement experimentally.

In our method we use only one grating without any moving, and thus making it proposed technique simpler and more convenient for implementation. The spatial information of the object is extracted from the Fourier transform of its spatial imaging. Our method allows obtaining reflectance or transmittance of a single or periodic object as a function of coordinate. Similarly to the temporal domain case, the object has to be spatially modulated. It can be done by a diffraction grating with known non-sinusoidal transmission or reflection profile, closely attached to the object. In our simulations, the object was taken to be a reflecting plane and the grating is transmitting. The light, passed trough the diffraction grating is reflected from the object with a certain reflection profile, then passing back trough the grating. Then the output plane of the diffraction grating is observed by a far-field microscope.

For simplicity, we restrict our consideration to one-dimensional object and incoherent illumination. Ideally, the spatial modulation has to be performed exactly in the plane of the object, and therefore the grating thickness ought to be infinitely small. The light intensity in the output plane of the diffraction grating can be written as

$$I_{\text{out}}(x) = R_{\text{ob}}(x)T_{\text{gr}}(x), \tag{10}$$

where x is the transverse coordinate, $R_{\text{ob}}(x)$ is the intensity reflection profile of the object, and $T_{\text{gr}}(x)$ is the grating's two-pass intensity transmittance. $R_{\text{ob}}(x)$ and $T_{\text{gr}}(x)$, taken in our simulations, are shown in Figs. 8 and 9, respectively. The grating period was chosen to be 230 nm. The periodic grating transmittance can be written as a Fourier series

$$T(x) = \sum_{n=-N}^{N} c_n \exp(2\pi i n x/\Lambda), \tag{11}$$

where c_n are the Fourier coefficients and Λ is the grating period. The object reflection $R_{\text{ob}}(x)$ can also be represented as a Fourier integral or a Fourier series for a non-periodic and periodic object, respectively. Physically, it implies that

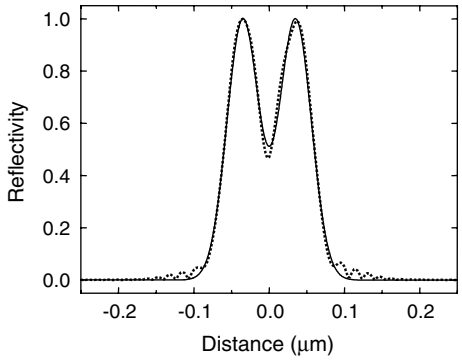

Fig. 8. Original (solid curve) and restored (dotted curve) reflection profile of the object.

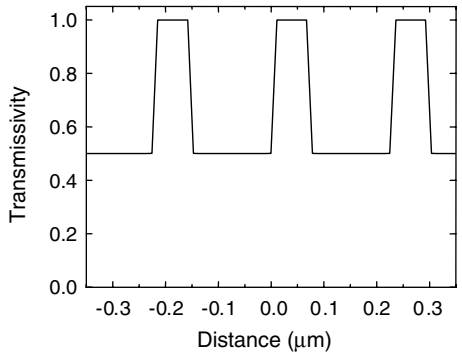

Fig. 9. Transmission profile of the periodic diffraction grating with a period of 230 nm.

we consider the object and the grating as two sets of infinite (or finite) number of closely attached sinusoidal gratings and the mechanism of the evanescent wave transformation is the same as in [18,19].

By substituting (11) to (10), taking into account the OTF of the imaging system, and performing a Fourier transform, we obtain an equation similar to Eq. (3) for the temporal domain

$$F_{\text{im}}(k_x) = H(k_x) \sum_{m=-N}^{N} c_{\text{m}} F_{\text{ob}}(k_x - m/\Lambda), \tag{12}$$

where k_x is the spatial frequency, $H(k_x)$ is the OTF of the system, $F_{\text{ob}}(k_x)$ and $F_{\text{im}}(k_x)$ are the Fourier transforms of the object reflectivity and the image of the modulated object, respectively. For simplicity, we assumed a system magnification $M_{\text{S}} = 1$. Eq. (12) has the same meaning as Eq. (3). As a result of modulation, the spatial spectrum of the object is shifted. If all of the shifted parts of the spectrum are within the system passband, the object spectrum can be restored by parts, according to the procedure, described above for the time domain. It can be seen from Fig. 10 that a significant part of the simulated object spatial spectrum is placed beyond the system passband. Therefore, without modulation and processing, we cannot see in the conventional far-field image in Fig. 11 two peaks spaced 60 nm apart that exist in the object, seen in Fig. 8.

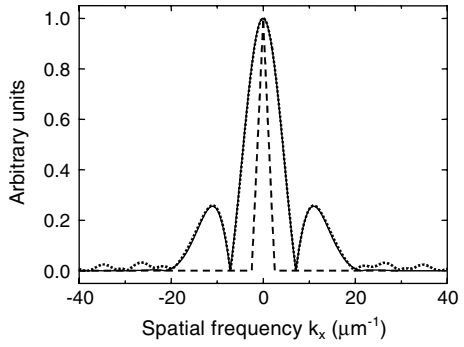

Fig. 10. Original (solid curve) and restored (dotted curve) intensity spectra of the object (Fourier transform of the object reflectivity). The OTF (dashed curve) of the imaging system.

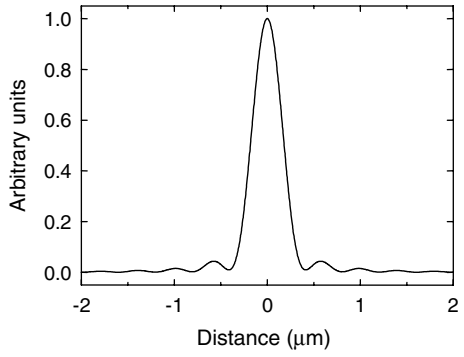

Fig. 11. Image of the object, shown in Fig. 8, by conventional (without modulation) far-field imaging system with the OTF, presented in Fig. 10.

We can use the same technique of the shifts between the object and modulation applied for the retrieval procedure in the time domain. In reality, the shifts of the grating relative to the object are difficult to implement. In simulations, we used the processing that does not require this shifting. If the object intensity spectrum is bounded, we can continue it periodically and expand into a Fourier series

$$F_{\mathrm{ob}}(k_x) = \sum_n d_n \exp(2\pi i n k_x/K), \tag{13}$$

where K and d_n are the period and the Fourier coefficients of the extended object spectrum, respectively. Eq. (12) can be rewritten in this case to give

$$F_{\mathrm{im}}(k_x) = H(k_x) \sum_n d_n \sum_{m=-N}^{N} c_{\mathrm{m}} \exp[-2\pi i n m/(K\Lambda)] \times \exp(2\pi i n k_x/K). \tag{14}$$

Solving the set of Eqs. (14) for the discrete values $k_x = s\Delta kx$ (s is the order number of sampling points, Δk_x is the sampling interval) we find d_n and then restore the Fourier transform of the object and the object itself. It is important to note that the period K ought to be sufficiently large so that there will not be overlaps of the shifted parts of the spectra related to adjacent periods. Our assumption regarding to the spectrum periodicity is equivalent to representation of the object as a sum of delta functions with a weight d_n for the nth delta. The interval between adjacent deltas is $1/K$. If the estimated full width of the object is Δx, we can estimate the number of the intervals between the deltas (sampling intervals in the space) as $K\cdot\Delta x$. The number of the unknowns d_n will be $K\cdot\Delta x + 1$. To obtain the same number of Eqs. (14) we divide the whole passband into $K\cdot\Delta x$ intervals. Thus, the sampling interval in the frequency space is $\Delta k_x = D/(K\cdot\Delta x)$, where D is the passband width.

We took for the simulations: $\Delta x \approx 0.3$ μm, $K = 120$ μm^{-1}. The passband width D of the system can be estimated as $D \sim 2/\lambda$. It is clear that the value of D should be as high as possible. We chose $D = 5$ μm^{-1} that corresponds to $\lambda = 0.4$ μm. Thus we can obtain the number of unknowns $K\cdot\Delta x + 1 = 37$ and the sampling interval $\Delta k_x = 0.139$ μm^{-1}. Finding the Fourier coefficients d_n, we restore the object spectrum according to Eq. (13). It can be seen from Fig. 10 that the original and restored spectra differ only at the wings. However, even that discrepancy can be eliminated by increasing the period K. The spatial distribution of the object is calculated from the inverse Fourier transform of the object spectrum. The restored object reflectivity is shown in Fig. 8 (dotted curve) along with the original object reflectivity (solid curve). We can see an excellent agreement.

Solution (13), (14) is exact for a strictly bounded spectrum. However, even in this case the reconstruction of the spectrum according to Eqs. (13) and (14) requires for the calculations high accuracy. This implies that small level of noise can affect the restored spectrum and drastically distort the image. We thus propose a solution which can provide more stability against noise.

First, we remind that in our method we divide the whole spectrum of the object into parts (bands), each having a width of $1/\Lambda$. The measurements can be made only within the central band and the spectrum should be restored in all of the bands. In each ith band, we represent the object spectrum as a polynomial

$$f_i(k_x) = \sum_{m=1}^{M} b_{\mathrm{im}} k_x^m, \tag{15}$$

where M is the number of sampling points in each band, $i = 0, \pm1, \pm2, \ldots, \pm N$, and $2N+1$ is the number of the bands. The total number of the sampling points is $(2N+1)M$. Then we replace the spectrum $F_{\mathrm{ob}}(k_x)$ in Eq. (12) by the functions $f_i(k_x)$ from (15)

$$F_{\mathrm{im}}(n\Delta k_x) = H(n\Delta k_x) \sum_{m=-N}^{N} c_{\mathrm{m}} f_{\mathrm{m}}(n\Delta k_x - m/\Lambda), \tag{16}$$

where $n\Delta k_x$ is the sampled value of k_x (n is an integer). Note that the sampled values of the image spectrum $F_{\mathrm{im}}(k_x)$ can be experimentally obtained only within the central passband having M sampling points. This means that according to (16) we can write M equations. We obtain the next set of $(2N+1)M$ equations from the condition

of equality of each function $f_i(k_x)$ in the sampling points of the ith band to the object spectrum expressed by (13). We also use the condition that the spectrum (13) is equal to 0 for the points between the spectrum periods such that the number of equations is equal to the number of unknowns, d_n and b_{im}.

First, we performed simulations in the absence of noise for the same object and the OTF shown in Figs. 8 and 10, respectively. We took the following parameters: $K = 76\ \mu\mathrm{m}^{-1}$, $M = 11$, $N = 5$, and the number of the Fourier coefficients d_n in (13) was 23. The restored spectrum and object completely coincide with the original ones in the plots. Therefore, we do not show them in the figures. It can be seen from Table 1 that the mean square deviation between the original and the restored objects is 0.3% in the absence of noise.

Now we include additive noise. We introduce additional $(2N+1)M$ unknowns Φ_{ik}, which are the sampled values of the image spectrum. i and k denote the order number of the band and of the sampling point in the band, respectively. Φ_{ik} deviates from the true values of the image spectrum at certain sampling points owing to noise. We require that the curves $f_i(k_x)$ fit the noisy points Φ_{ik} in each ith band according to the least mean square method. It gives additional $(2N+1)M$ equations. The relation between the bands given by (16) ought to be rewritten now for the random values Φ_{ik}.

$$F_{\mathrm{im}}(n\Delta k_x) = H(n\Delta k_x)\sum_{m=-N}^{N} c_{\mathrm{m}}\Phi_{mn}. \tag{17}$$

$F_{\mathrm{im}}(n\Delta k_x)$ in (17) is the sampled values of the noisy spectrum within the central band obtained from the noisy object by a Fourier transform. By solving all of the equations simultaneously we obtain the values of Φ_{ik}, d_n, and b_{im}.

In the simulations, we modeled the noise by generation of normally distributed random numbers with a zero mean value and a given standard deviation. The noise was added to the object (the same object as in Fig. 8) and then the noisy image spectrum was calculated. We took the same parameters that were used in the noiseless case. We calculated the root-mean-square (rms) deviation between the original and restored objects as a function of the noise level (standard deviation). The maximal value of the object reflectivity taken in the simulations was unity. Results of the calculation are shown in Table 1. It can be seen that up to a noise level of 10^{-2} (1% from the maximal value of the object reflectivity) the rms deviation does not depend practically on the noise. For a noise level of 3×10^{-2} the deviation increases up to 13.9% and then for a noise level larger than 5×10^{-2} the restored object is absolutely different from the original one. In Figs. 12 and 13 we show the restored spectrum and object, respectively, in comparison with the original ones for a noise level of 10^{-2}. We see that the solution is much more stable against noise fluctuations.

The advantage of our method in that only a single measurement of the object image ought to be performed for the retrieval process instead of the multiple shifts and measurements in the temporal domain. This possibility is important because shifting a diffractive element in the spatial domain is difficult to implement. For the temporal domain one can choose one of these two methods. The first one with multiple measurements is more complex, but more resistant against noise compared to the second method. The second one with a single measurement is simpler to implement but requires more complicated processing.

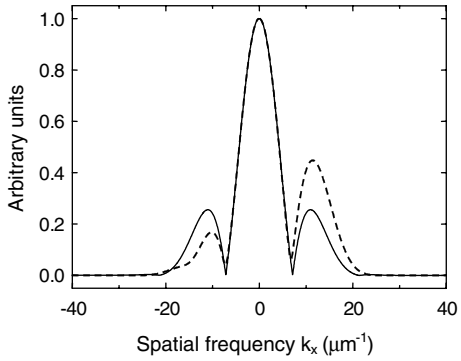

Fig. 12. Original (solid curve) and restored (dashed curve) intensity spectra of the object in the presence of the noise with a level of 0.01 (1% from the maximal value of the object reflectivity).

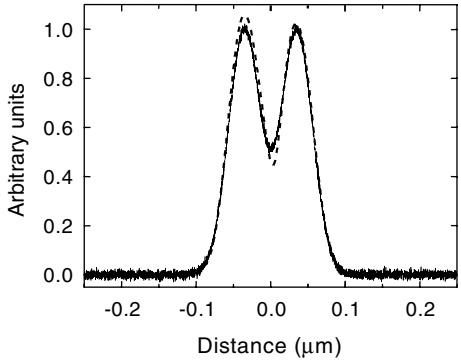

Fig. 13. Original (solid curve) and restored (dashed curve) reflection profile of the object in the presence of noise obtained from the restored spectrum shown in Fig. 12.

Table 1
Dependence on the noise level of the root-mean-square deviation of the restored object from the original one

Noise level	0	10^{-8}	10^{-7}	10^{-6}	10^{-5}	10^{-4}	10^{-3}	10^{-2}	3×10^{-2}	5×10^{-2}
rms deviation (%)	0.32	4.8	4.8	4.8	4.9	4.6	5.1	3.4	13.9	>100

It should be taken into account that in reality the thickness of the grating cannot be infinitely small. Then, our approximation is valid if for the highest harmonic order of the grating profile used in the processing, the distance of the evanescent waves decay is much larger than the grating thickness. This condition determines the maximal resolution achievable by the method. Other aspects are the way real diffraction grating follows Eq. (10), and the accuracy of the grating profile (transmission or reflection) measurement that also affects the subwavelength resolution. The calibration has to be done with a near-field microscope. For our simulation, the spatial resolution of such calibration ought to be about 10 nm.

5. Conclusion

We have presented a method that allows the retrieval of optical pulse waveforms even when the intensity spectrum is much wider than the passband of the measuring system. The pulse shape can be restored by using temporal intensity modulation. We are able by this technique to increase effectively the passband of the measuring oscilloscopes and photodetectors beyond usually available bandwidths that are about 50–70 GHz. The simple processing allows one to obtain the measured pulse waveform in real time. Another advantage compared to temporal or spectro-temporal imaging techniques is that we do not need here any dispersive elements that substantially complicate the waveform measurement. No conditions are imposed on the temporal modulation except the need of high harmonics. The method becomes very simple for periodic pulses with high duty cycle where even the need of an oscilloscope is relaxed. Only a few measurements by a power meter after the appropriate pulse train shifts are needed for the pulse waveform recovery.

We also showed that the method can also be applied for the spatial case, achieving subwavelength spatial resolution in far-field microscopy. The spatial modulation is performed, for instance, by a diffraction grating. The grating also transforms evanescent waves that carry subwavelength information to propagating waves. The method allows reconstructing subwavelength objects only from one measurement, without shifting them relative to the grating. Our technique does not need a second grating for decoding the spatial information about an object. This information is extracted from the Fourier transform of the object image. The object reconstruction ambiguity is resolved since the processing is based on the image spectrum beyond the system passband. The spectrum extension is provided by the spatial modulation of the grating.

References

[1] C.V. Bennett, B.H. Kolner, Opt. Lett. 24 (1999) 783.
[2] J. Azaña, N.K. Berger, B. Levit, B. Fischer, IEEE Photon. Technol. Lett. 17 (2005) 94.
[3] M.T. Kauffman, W.C. Banyai, A.A. Godil, D.M. Bloom, Appl. Phys. Lett. 64 (1994) 270.
[4] L.K. Mouradian, F. Louradour, V. Messager, A. Barthélémy, C. Froehly, IEEE J. Quantum Electron. 36 (2000) 795.
[5] J. Azaña, N.K. Berger, B. Levit, B. Fischer, IEEE Photon. Technol. Lett. 16 (2004) 882.
[6] Y.M. El-Batawy, M.J. Deen, J. Lightwave Technol. 23 (2005) 423.
[7] M.G.L. Gustafsson, J. Microsc. 198 (2000) 82.
[8] R. Heintzmann, T.M. Jovin, C. Cremer, J. Opt. Soc. Am. A 19 (2002) 1599.
[9] M.G.L. Gustafsson, Proc. Natl. Acad. Sci. USA 102 (2005) 13081.
[10] B.H. Kolner, IEEE J. Quantum Electron. 30 (1994) 1951.
[11] J.L. Harris, J. Opt. Soc. Am. 54 (1964) 931.
[12] C.K. Rushforth, R.W. Harris, J. Opt. Soc. Am. 58 (1968) 539.
[13] W. Lukosz, J. Opt. Soc. Am. 56 (1966) 1463.
[14] W. Lukosz, M. Marchand, Opt. Acta 10 (1963) 241.
[15] D. Mendlovic, A.W. Lohmann, N. Konforti, I. Kiryuschev, Z. Zalevsky, Appl. Opt. 36 (1997) 2353.
[16] J.M. Vigoureux, D. Courjon, Appl. Opt. 31 (1992) 3170.
[17] H. Nassenstein, Opt. Commun. 2 (1970) 231.
[18] J.M. Guerra, Appl. Phys. Lett. 66 (1995) 3555.
[19] V. Eckhouse, Z. Zalevsky, N. Konforti, D. Mendlovic, Opt. Eng. 43 (2004) 2462.
[20] M.A. Grimm, A.W. Lohmann, J. Opt. Soc. Am. 56 (1966) 1151.
[21] D. Marks, P.S. Carney, Opt. Lett. 30 (2005) 1870.